

# Constrained simulations of the local universe: II. The nature of the local Hubble flow

Luis A. Martínez-Vaquero<sup>1</sup>, Gustavo Yepes<sup>1</sup>, Yehuda Hoffman<sup>2</sup>, Stefan Gottlober<sup>3</sup>, Mira Sivan<sup>2</sup>

<sup>1</sup>Grupo de Astrofísica, Universidad Autónoma de Madrid, Madrid E-280049, Spain

<sup>2</sup>Racah Institute of Physics, Hebrew University, Jerusalem 91904, Israel

<sup>3</sup>Astrophysikalisches Institut Potsdam, An der Sternwarte 16, 14482 Potsdam, Germany

21 February 2024

## ABSTRACT

Using a suite of  $N$ -body simulations in different Cold Dark Matter (CDM) scenarios, with cosmological constant ( $\Lambda$ CDM) and without ( $\Lambda$ CDM, SCDM), we study the Hubble flow ( $H_H$ ) in Local Volumes (LV) around Local Group (LG) like objects found in these simulations, and compare the numerical results with the most recent observations. We show that  $\Lambda$ CDM and  $\Lambda$ CDM models exhibit the same behavior of  $H_H$ . Hence, we demonstrate that the observed coldness of the Hubble flow is not likely to be a manifestation of the dark energy, contrary to previous claims. The coldness does not constitute a problem by itself but it poses a problem to the standard  $\Lambda$ CDM model only if the mean density within the Local Volume is greater than twice the mean matter cosmic density. The lack of blueshifted galaxies in the LV, outside of the LG can be considered as another manifestation of the coldness of the flow. Finally, we show that the main dynamical parameter that affects the coldness of the flow is the relative isolation of the LG, and the absence of nearby Milky Way like objects within a distance of about 3M pc.

**Key words:** methods: numerical { galaxies: Local Group { cosmology: dark matter

## 1 INTRODUCTION

The neighborhood of the Local Group (LG) is often described as being cold. This attribute implies that the dispersion of the radial velocities of galaxies from a pure Hubble flow is small, and the ‘smallness’ amounts to less than  $100 \text{ km s}^{-1}$ . Sandage et al. (1972) studied local departures from a uniform Hubble flow and could only put upper limits on such departures. This led Sandage et al. to conclude that  $q_0 < 0$  (where  $q_0$  is the deceleration parameter). Later on Sandage & Tamman (1975) estimated that the upper limit to the mean random motion of field galaxies is  $\sim 50 \text{ km s}^{-1}$ . These early findings of Sandage, Tamman and their collaborators have been corroborated and vigorously improved by many others. Karachentsev et al. (2003) estimated the radial peculiar velocity dispersion of all galaxies within 5.5M pc to be  $85 \text{ km s}^{-1}$ . This value drops down to  $41 \text{ km s}^{-1}$  if members of galaxy groups are removed and distance errors are taken into account. Using a newer set of Karachentsev’s data Tikhonov & Klypin (2008) found a velocity dispersion of  $97 \text{ km s}^{-1}$ , within 7M pc, which reduces after correction for apex motion and distance errors only slightly to  $84 \text{ km s}^{-1}$ . Macciò et al. (2005) compiled the data

from three different sources: The Cepheid-based distance measurements of the HST Key Project (Freedman et al. 2001), distance estimates based on the surface brightness fluctuations method (Tonry et al. 2001) and Tully-Fisher distances (Tully et al. 1992). They fitted the data by  $H_H = 88 \pm 20 \text{ km s}^{-1} (R = 7 \text{ M pc})$ , where  $H_H$  is a measure of the dispersion of the radial velocities around a pure Hubble flow of galaxies within a sphere of radius  $R$  (a thorough discussion of the various estimates of  $H_H$  is given below).

The observational evidences for a local cold Hubble flow seem to be indisputable. Yet, the question arises as to why a  $H_H$  of the order of a few tens of  $\text{km s}^{-1}$  is labeled as ‘cold’. Namely, by what standard is it cold?. Rich clusters of galaxies provide the first and the most robust evidence for a departure from a pure Hubble flow, with a dispersion of peculiar velocities of up to  $10^3 \text{ km s}^{-1}$ . Compared with the rich clusters the neighborhood of the LG is definitely cold. A statistical estimate is also given by the pairwise velocity dispersion ( $\sigma_{12}$ ) which was measured from the CfA redshift survey to be  $\sigma_{12}(r = 1 \text{ h}^{-1} \text{ M pc}) = 340 \pm 40 \text{ km s}^{-1}$  (Davis & Peebles 1983). Another more robust measure of the deviation from the Hubble flow is provided by the  $\chi^2$  statistics

which measures the one-dimensional rms peculiar-velocity dispersion of galaxies relative to their neighbors within a projected radius of  $2h^{-1}Mpc$  (Davis, Miller & White 1997). These authors found  $\sigma_1 = 95 \pm 16 km s^{-1}$  (for the IRAS survey) and  $130 \pm 15 km s^{-1}$  for the UGC catalog. The measured  $\sigma_1$  is indeed much ‘hotter’ than the  $\sigma_H = 25 km s^{-1}$  within  $R = 3.0Mpc$  (Karachentsev et al. 2009). So, with regard to the other measure of the dispersion of peculiar velocities the immediate neighborhood of the LG is indeed very cold. However, one should recall that the  $\sigma_1$  and  $\sigma_2$  measures consider all galaxies in a given survey. The  $\sigma_H$  considered here, on the other hand, refers to one particular object, namely the LG, that resides in a dynamically quiet environment. It should be emphasized that the LG is not an atypical object, yet the LG environment is not a representative one for Milky Way like objects. This implies that, when addressing the issue of ‘coldness’ by means of simulations, the selection of the LG-like objects should be carefully done.

The standard model of cosmology consists of a flat Friedmann universe whose mass energy is dominated by a cosmological constant ( $\Lambda$ ) and cold dark matter (labeled as  $\Lambda$ CDM). It has been recently stated that the cosmological constant, or its generalization the Dark Energy (DE), manifests itself in the dynamics of the very local universe (Baryshev et al. 2001, Chemin et al. 2004, 2007). These authors argued that the coldness of the local flow is a manifestation of the existence of the dark energy. This has been supported by Maccio et al. (2005) who analysed a set of  $N$ -body simulations and concluded that indeed “.. [their] results provide new, independent evidence for the presence of dark energy on scales of a few megaparsecs”. These results, if correct, would have provided an independent corroboration to the DE component whose existence is otherwise inferred from observations of distant objects and on very large scales of the Universe. The claims of Chemin et al. (2007) have been challenged by Ho man et al. (2008), who analyzed a suit of constrained and unconstrained  $\Lambda$ CDM simulations, identified LG-like objects and studied the flow field around these. The main result of Ho man et al. (2008) invalidates the model advocated by Chemin et al. (2007) and its basic predictions. The claim made by Maccio et al. (2005) have remained unchallenged till present.

There are two main issues this paper addresses. The claim that the coldness of the local flow is induced by the dark energy, and the fact that it is strongly contradicted by Ho man et al. (2008), motivated us to revisit the problem. Then, there is the general problem of the nature of the local flow. In particular the question of how the various characteristics of the local neighborhood are affecting the local flow is addressed here.

The present paper adopts the methodology used by Maccio et al. (2005) and later on by Ho man et al. (2008). Namely, a set of numerical simulations is performed, ensembles of LG-like objects are constructed and  $\sigma_H$  is calculated around these mock objects in the same way as the Hubble flow around the actual LG is analyzed. This is further extended here. The cosmological models studied here are the presently accepted model of cosmology with a cosmological constant,  $\Lambda$ CDM, the open  $\Lambda$ CDM ( $\Omega$ CDM) and the outdated Einstein-De Sitter SCDM models (where S stands for the standard of the years of the 1990s and CDM stands for cold dark matter). Most of the simulations studied here

are constrained and thereby are constructed to reproduce within the simulation box the observed Large Scale Structure (LSS) on scales larger than  $5h^{-1}Mpc$ . A thorough study of the nature of the local Hubble flow is done by studying the dependence of  $\sigma_H$  on a multitude of factors, including the cosmological parameters, the mass resolution, the very local environment and the structure on larger scales. The control over the very small scales is achieved by varying the selection rules for the LG-like objects and the control over the large scale environment is done by performing the constrained simulations. A somewhat different selection of mock objects is obtained by constraining them to have no nearby blueshifted galaxies.

The structure of the paper is as follows. A summary of the CNG data and examination of the different ways of calculating  $\sigma_H$  are given in x2. x3 describes the  $N$ -body simulations analyzed here and a description of the selection of the LG-like objects is presented in x4. The analysis of  $\sigma_H$  is conducted first along the lines of Maccio et al. (2005) (x5). Then the dependence of  $\sigma_H$  on the various characteristics of the LG is shown in x6 and the possible role of mass resolution, in x7. The lack of nearby blueshifted galaxies as a manifestation of the coldness of the local flow is analyzed in x8. The paper concludes with a summary and a general discussion (x9).

## 2 OBSERVATIONS

The Catalog of Neighboring Galaxies (Karachentsev et al. 2004, CNG) provides the latest and most comprehensive survey of the velocities of nearby galaxies. The catalog includes the distances and radial velocities of more than 400 galaxies, roughly 300 of which are in the Local Volume (LV), defined by a sphere of  $R = 7Mpc$  about the LG. Tikhonov & Klypin (2008) have recently compiled the catalog and calculated  $\sigma_H$  of all the CNG galaxies within the LV. Distances are typically measured with 10% errors. Tikhonov & Klypin studied the recent, yet unpublished version of the catalog. That compilation of the data is taken here as the observational reference value, against which our numerical results are to be compared.

The local flow is studied here within the framework defined by Tikhonov & Klypin (2008). Their study ignores non-linear motions within the LG and therefore all galaxies closer than  $1.0Mpc$  are excluded from the analysis. The flow is analyzed by means of measuring the dispersion of the radial velocities about the Hubble flow of all galaxies found within the LV, which is redefined to correspond to the shell of  $(1 \pm 7)Mpc$ . The choice to consider all galaxies regardless of their possible membership in galaxy groups is driven by the principle of keeping the selection to be as clear and simple as possible. This avoids the issue of defining a galaxy group catalog and simplifies the comparison of observations and simulations.

There are different ways of defining the scatter of the line-of-sight (LOS) velocities from a pure Hubble,  $\sigma_H$ . Consider a catalog of galaxies whose distances and radial velocities are measured,  $f(x_i; v_i)_{i=1, \dots, N}$ . Tikhonov & Klypin (2008) estimated the apex motion of the observer, namely the LG, with respect to the sample of galaxies in the catalog and subtracted the apex velocity from the observed LOS

velocities. The dispersion  $\sigma_H$  is then calculated as the root mean square (RMS) with respect to the Hubble flow, where the global value of the Hubble constant ( $H_0$ ) is assumed. Maccio et al. (2005) defined  $\sigma_H$  by the standard deviation (SDV) of the residual LOS velocities. This is equivalent to measuring the RMS of the residual velocities from the local Hubble flow, namely using the locally determined Hubble constant from the data itself ( $H_{loc}$ ). Yet, a simpler approach is to associate  $\sigma_H$  with the RMS of the residual from the global Hubble flow. This is the approach adopted here, namely  $\sigma_H$  is calculated by:

$$\sigma_H^2 = \frac{1}{N} \sum_{i=1}^N [v_i - H_0 r_i]^2 \quad (1)$$

and the sum extends over the  $N$  galaxies within the appropriate distance cut of the catalog. Hereafter these methods are referred to as the APEX, SDV and RMS.

One can argue for the merits and disadvantages of the different methods and they all can be used as long as observations and simulations are analyzed consistently. Still, we argue here that the use of the dispersion around the global Hubble flow is the preferred way. The motivation for measuring  $\sigma_H$  stems from the information it provides on the deviations from a pure Hubble flow. By using the locally determined Hubble constant the ‘breathing’ (i.e. isotropic) mode of the flow is absorbed in  $H_{loc}$ , and so the resulting  $\sigma_H$  underestimates the actual deviation from a pure Hubble flow. In the case of the apex motion the velocity of the LG, that hosts the observer, is treated as if it is an external effect that is not related to the perturbed flow one is trying to study. It is solved in a manner which does not depend on the nature of the perturbation field. The inclusion of the apex motion of the observers provides a better measure of the deviation from a pure Hubble flow. Yet, it is shown here that the differences between the different measures are small. The different measures of  $\sigma_H$  have been applied to an ensemble of LG-like objects drawn from one of the high resolution simulations studied here (CDM hr, see x3 for a detailed description). Figure 1 presents the results obtained for the different estimators of  $\sigma_H$ . The main result is that the differences between the different methods are much smaller than the scatter around the median of calculated values of  $\sigma_H$ .

Table 2 of Tikhonov & Klypin (2008) provides the RMS and APEX estimates of  $\sigma_H$  for the CNG galaxies for various radial cuts. These estimates are corrected for distance errors. The representative number used here is the RMS estimation for all galaxies within (1–7) Mpc of  $\sigma_H = 90.4 \text{ km s}^{-1}$ .

### 3 SIMULATIONS

A suit of constrained and unconstrained CDM (at, and CDM),  $\Lambda$ CDM (open, CDM only) and SCDM (at, CDM only) low and high resolution simulations have been performed. Table 1 lists the names and the parameters of the simulations. The low resolution simulations ( $N = 256^3$ ) are the same ones described in Martínez-Vaquero et al. (2007) and Ho man et al. (2008). A computational box of  $L = 64 h^{-1} \text{ Mpc}$  (where  $h$  is Hubble’s constant in units of  $100 \text{ km s}^{-1} \text{ Mpc}^{-1}$ ) and the WMAP1 cosmological parameters are assumed for the CDM simulations (Spergel et al.

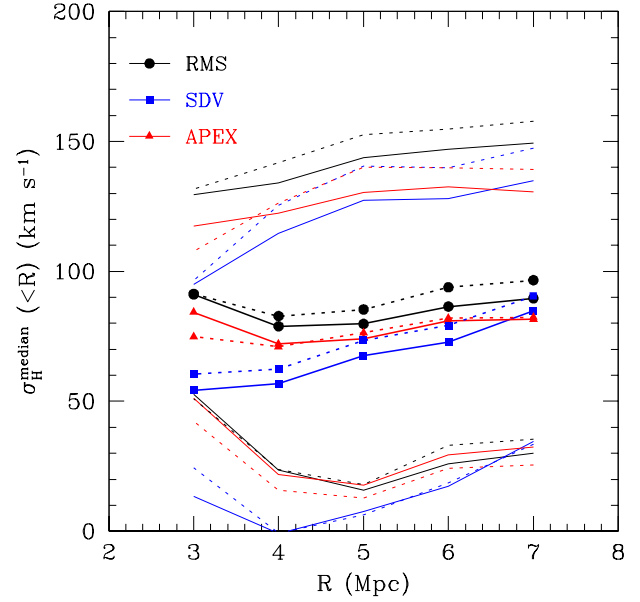


Figure 1. The median of  $\sigma_H$  (lines with points) and its standard deviation (thin lines) for the CDM hr simulation taking all the DM halos (solid lines) and only those with a circular velocity higher than  $35 \text{ km s}^{-1}$  (dotted lines) in the distance range of (1– $R$ ) Mpc computed using the APEX (triangles), SDV (squares) and RMS (circles) methods.

2003). The  $\Lambda$ CDM simulations are identical to the CDM ones but without the  $\Lambda$  term, hence they correspond to an open universe. The SCDM is used here just as an extreme model for which the Hubble flow is expected to be much hotter than all other models, despite the fact that is a cosmological model which stands in marked disagreement with a wide range of cosmological observations. The low resolution, constrained and unconstrained, simulations are all based on the same realization of the Gaussian random field. The CDM hr and CDM 160 are high resolution ( $N = 1024^3$ ) simulations in computational boxes of  $L = 64$  and  $160 h^{-1} \text{ Mpc}$  respectively. Both are performed with the WMAP3 cosmological parameters (Spergel et al. 2007).

Five of the simulations are constrained ones, namely the initial conditions of these are set by constrained realizations of Gaussian fields. Observational data of the nearby universe is used as constraints on the initial conditions and thereby the resulting simulations reproduce the observed LSS. The basic algorithm of constraining Gaussian random fields is the one developed by Ho man & Ribak (1991). The implementation of the algorithm to observational data and a description of the construction of constrained simulations was described at length in Kravtsov et al. (2002) and Klypin et al. (2003). A brief description of the constraining data is given here. Two different observational data is used to set up the initial conditions. The first is made of radial velocities of galaxies drawn from the MARK III (Willick et al. 1997), SBF (Tonry et al. 2001) and the Karachentsev et al. (2004) catalogs. Peculiar velocities are less affected by non-linear effects and are used as constraints as if they were linear quantities (Zaroubi et al. 1999). The other constraints are obtained from the catalog of nearby X-ray selected clusters

of galaxies (Reiprich & Bohringer 2002). Given the virial parameters of a cluster and assuming the spherical top-hat model one can derive the linear overdensity of the cluster. The estimated linear overdensity is imposed on the mass scale of the cluster as a constraint. For the  $\Lambda$ CDM cosmologies the data used here constrains the simulations on scales larger than  $5 h^{-1} \text{Mpc}$  (Klypin et al. 2003). It follows that the main features that characterize the local universe, such as the Local Supercluster, Virgo cluster, Coma cluster and Great attractor (in the large box), are all reproduced by the simulations. The small scale structure is hardly affected by the constraints and is essentially random.

We have used the parallel TREEPM N-body code GADGET2 (Springel 2005) to run these simulations. A uniform mesh of  $512^3$  grid points was used to compute the long-range gravitational force by means of the Particle-Mesh algorithm. A constant comoving Plummer equivalent gravitational smoothing scale of  $20 h^{-1} \text{kpc}$  was set at high redshift and we changed it to  $5 h^{-1} \text{kpc}$  physical scale since  $z=3$  till  $z=0$ . The simulations were started at  $z=50$  in all cases. We employed a variety of parallel computer architectures (SG I-ALIX, IBM-SP4, Opteron-clusters) during the course of this work. Using 16 processors simultaneously, we completed one run in about 2 cpu days.

We analyzed also two simulations with higher mass resolution ( $1024^3$  particles). The simulation with box size  $64 h^{-1} \text{Mpc}$  has been also evolved using GADGET2. A grid of  $1024^3$  was used in this case for the computation of the PM forces. Gravitational smoothing was set to  $1.6 h^{-1} \text{kpc}$  at high redshift and  $0.8 h^{-1} \text{kpc}$  at lower redshift. The initial conditions were set up at  $z=100$  for this run. The simulation of box size  $160 h^{-1} \text{Mpc}$  has been calculated by the MPI version of the Adaptive Renement Tree (ART) code described in Gottlober & Klypin (2008). Initial conditions were set up at  $z=30$  and the maximum number of renement levels were set to 9, which translates into a maximum spatial resolution of  $1.2 h^{-1} \text{kpc}$ . These two high resolution simulations were also analyzed by Tikhonov & Klypin (2008).

We conclude this section with a general remark. The parameters of the simulations are defined by using the  $h^{-1}$  scaling. Yet, the comparison of the results with observations, and in particular the distance cuts, is made after an  $H_0 = 73 \text{ km s}^{-1} \text{Mpc}^{-1}$  is assumed and distances are expressed in units of "real" Mpc.

#### 4 SELECTION OF LG CANDIDATES

DM halos were found in simulations using two object finding methods: The Bound Density Maximum (BDM) algorithm (Klypin et al. 1999) is based on finding local center of mass in spheres of variable radius starting from randomly selected particles in the simulation. The AMIGA Halo Finder (Gillet et al. 2004), on the contrary, finds local density maximum from an adaptive mesh hierarchy. In both cases, an iterative procedure to find local centre of mass from density maximum is used. Particles that are gravitationally unbound to the halo potential are also removed. Only halos with a mass higher than  $2.6 \cdot 10^{10}$  ( $\Lambda$ CDM,  $\Lambda$ CDM<sub>u</sub>,  $\Lambda$ CDM and  $\Lambda$ CDM<sub>u</sub>),  $8.7 \cdot 10^{10}$  (SCDM),  $5.0 \cdot 10^8$  ( $\Lambda$ CDM<sub>hr</sub>) and  $4.0 \cdot 10^9 M_\odot$  ( $\Lambda$ CDM 160) are considered. For the work re-

ported here we have used the halo catalogues obtained by the AMIGA code, except for the  $\Lambda$ CDM 160 simulation where we have used the BDM halo catalogue. In any case, we have checked that the results are independent of the halo finder.

One of the main aims of this paper is to perform a detailed comparison with Maccio et al. (2005) results, so as to be able to challenge their claim on the role of the DE in the local dynamics. In order to meet this goal the selection criteria of LG-like objects of Maccio et al. have been followed to the letter. Going beyond the comparison with that paper the selection rules are reexamined and some of which are revised. Here, these criteria are expressed in physical units without the  $h^{-1}$  scaling. The LG objects obey the following selection:

- (i) The groups contain two MW and M31 like DM halos with maximum circular velocity in the range of  $125 \leq V_c \leq 270 \text{ km s}^{-1}$ .
- (ii) The two major DM halos are separated by no more than 1Mpc.
- (iii) The relative radial velocity of the two main halos is negative.
- (iv) There are no objects with maximum circular velocity higher than MW and M31 candidates within a distance of 3Mpc.
- (v) The group resides within a distance of 7 to 17Mpc from one and only one Virgo like halo of  $500 \leq V_c \leq 1500 \text{ km s}^{-1}$ . No Virgo like halos can appear within a distance of 7Mpc.

The selected LG-like objects obeying all the above rules are defined as Pairs, for the fact that they are dominated by two MW and M31 like DM halos.

A careful examination of the dynamics of LG-like objects suggests the dynamics of the Hubble flow might not depend strongly on whether they are dominated by two, almost equal, massive objects or by rather one massive objects (see Maccio et al. 2005 and Tikhonov & Klypin 2008). To test this idea we construct the Singles ensemble of LG-like objects which obey all the criteria presented above apart from the first one. Namely, for the Singles objects we look for individual halos, whose mass are similar to MW and M31 together, namely  $10^{12} \leq M_{\text{vir}} \leq 2 \cdot 10^{12} h^{-1} M_\odot$ . The LV around such objects is studied.

In Table 2, the number of LG candidates found following both criteria is shown. Higher number of LG-like objects are obtained using Singles criterion because it is less restrictive than the Pairs one. One should note that there is not a one-to-one correspondence of mock LGs in the  $\Lambda$ CDM and  $\Lambda$ CDM simulations, even if they have the same computational box and random realization of the initial conditions. This stems for the fact that the LG constitutes a quasi-linear object, far from being in virial equilibrium. LG-like objects are delicately defined to match the observed LG and the small dynamical differences introduced by the term are likely to prevent a full correspondence between objects in the different models.

Some of the simulations used here are constrained ones, namely their large scale structure is constrained to reproduce the observed cosmological neighborhood. No attempt is made here to select only LG-like objects that reside in the 'correct' position within the cosmic web that constitutes the local neighborhood, as this would result in a very poor statis-



| MODEL   | CONSTRAINED | BOX [h <sup>-1</sup> M pc] | m    | h    | g    | N    | m <sub>DM</sub> [h <sup>-1</sup> M <sub>⊙</sub> ] |                     |
|---------|-------------|----------------------------|------|------|------|------|---|---------------------|
| CDM     | yes         | 64                         | 0.30 | 0.70 | 0.70 | 0.90 | 256 <sup>3</sup>                                  | 1:3 10 <sup>9</sup> |
| CDM u   | no          | 64                         | 0.30 | 0.70 | 0.70 | 0.90 | 256 <sup>3</sup>                                  | 1:3 10 <sup>9</sup> |
| CDM hr  | yes         | 64                         | 0.24 | 0.76 | 0.73 | 0.75 | 1024 <sup>3</sup>                                 | 1:6 10 <sup>7</sup> |
| CDM 160 | yes         | 160                        | 0.24 | 0.76 | 0.73 | 0.75 | 1024 <sup>3</sup>                                 | 2:5 10 <sup>9</sup> |
| OCDM    | yes         | 64                         | 0.30 | 0    | 0.70 | 0.90 | 256 <sup>3</sup>                                  | 1:3 10 <sup>9</sup> |
| OCDM u  | no          | 64                         | 0.30 | 0    | 0.70 | 0.90 | 256 <sup>3</sup>                                  | 1:3 10 <sup>9</sup> |
| SCDM    | yes         | 64                         | 1.0  | 0    | 0.50 | 0.7  | 256 <sup>3</sup>                                  | 4:4 10 <sup>9</sup> |

Table 1. Description of the set-up and cosmological parameters used for the different simulations: constrained or random, computational box size, matter density ( $\rho_m$ ), cosmological constant ( $\Lambda$ ), Hubble’s constant ( $h$ ), initial power spectrum normalization ( $g$ ), number of particles ( $N$ ) and mass of the DM particle ( $m_{DM}$ )

| Criterion | CDM | CDM u | CDM hr | CDM 160 | OCDM | OCDM u | SCDM |
|-----------|-----|-------|--------|---------|------|--------|------|
| Pairs     | 13  | 20    | 12     | 131     | 11   | 15     | 24   |
| Singles   | 52  | 65    | 43     | 478     | 38   | 60     | 78   |

Table 2. Number of LG candidates found in each simulation following the Pairs and Singles criteria.

tics. Rather, objects are defined as LG-like, Pairs or Singles, regardless of their location in the computational box, and the flow field around these objects is studied.

## 5 ANALYSIS OF HUBBLE FLOW WITH IN THE LOCAL VOLUME

The main purpose of the present section is to study the dispersion of the peculiar velocities around LG-like objects selected in the manner of Maccio et al. (2005). The flow around each object is studied using the RMS estimator of  $v_H$ , so as to allow a comparison with the analysis of the CNG data (Tikhonov & Karachentsev 2006). The analysis consists of three parts:

- The examination of the Hubble diagram of the flow around LG-like objects.
- The statistical distribution of  $v_H$  of the various models.
- The dependence of  $v_H$  on the mean density of the LV around each object.

In all cases we take a spherical shell of (1–7) M pc as the LV of each object and, unless otherwise stated,  $v_H$  corresponds to all objects within the LV. Like with the actual data, the inclusion or omission of halos within 1.0 M pc distance leaves the value of  $v_H$  virtually unchanged.

The six panels of Fig. 2 present the combined Hubble diagram of 10 randomly chosen LG-like objects of the different models. The solid line corresponds to the unperturbed Hubble flow and the upper and lower dashed lines corresponds to  $H_0 \pm v_H$ , where  $v_H$  is the median value of  $v_H$  for each simulation. The individual points with the error bars represent the value of  $v_H(R)$  from Tikhonov & Klypin (2008) observational data. The results from CDM hr simulation are not shown in Figures 2, 3 and 4 since they are very similar to the other CDM simulations.

Table 3 presents the mean  $v_H$  of the full LV taken over the Pairs and the Singles in each of the simulations. The fractional cumulative distribution,  $F(v_H) = N(< v_H)/N_T$ ,

is presented in Fig. 3, where  $N(< v_H)$  is the number of LG-like objects colder than  $v_H$  and  $N_T$  is the total number of LG objects. The cumulative distribution is shown for all models and for both the Pairs and the Singles. In each frame the vertical line indicates the observational value of  $v_H = 90.4 \text{ km s}^{-1}$  and the numbers give the fraction of LG-like objects with  $v_H$  smaller than the observed value of the Pairs and the Singles (in parentheses).

Fig. 3 shows that there is a large scatter in the distribution of  $v_H$  and that for all the models considered here there is a non-negligible probability to find LG-like objects with  $v_H$  equal or smaller than the one corresponding to the actual LG. However, there is another dynamical variable that controls the dynamics around these objects and that is the mean density within the LV. This was shown by Maccio et al. (2005) and it is clearly reproduced by the analysis of the models considered here. Fig. 4 shows the scatter plot of  $v_H$  vs. the mean matter density within the LV normalized by the mean cosmological density. Both Pairs and Singles LG-like objects are studied and the results are virtually the same in the range of  $\rho_{DM} = \rho_{DM,62}$ , where  $\rho_{DM}$  and  $\rho_{DM,62}$  are the mean DM density within the LV and the cosmological mean DM density. In the simulations the DM density is very easily measured but this is not a directly observable quantity. Observationally the galaxy distribution within the LV is used to infer a local density. Short of having numerical simulations with full galaxy formation treatment the density of DM halos is used here as a proxy to the galaxy distribution. The lower panel of Fig. 4 presents the dependence of  $v_H$  on the density of mass which belongs to halos within the LV normalized by the mean mass density of all the simulated volume. In both panels of Fig. 4 the horizontal line denotes the observational estimate of  $v_H$ .

## 6 RELAXING THE LOCAL GROUP CRITERIA

The LG appears to be a very typical small group of galaxies, whose main dynamical characteristics are summarized

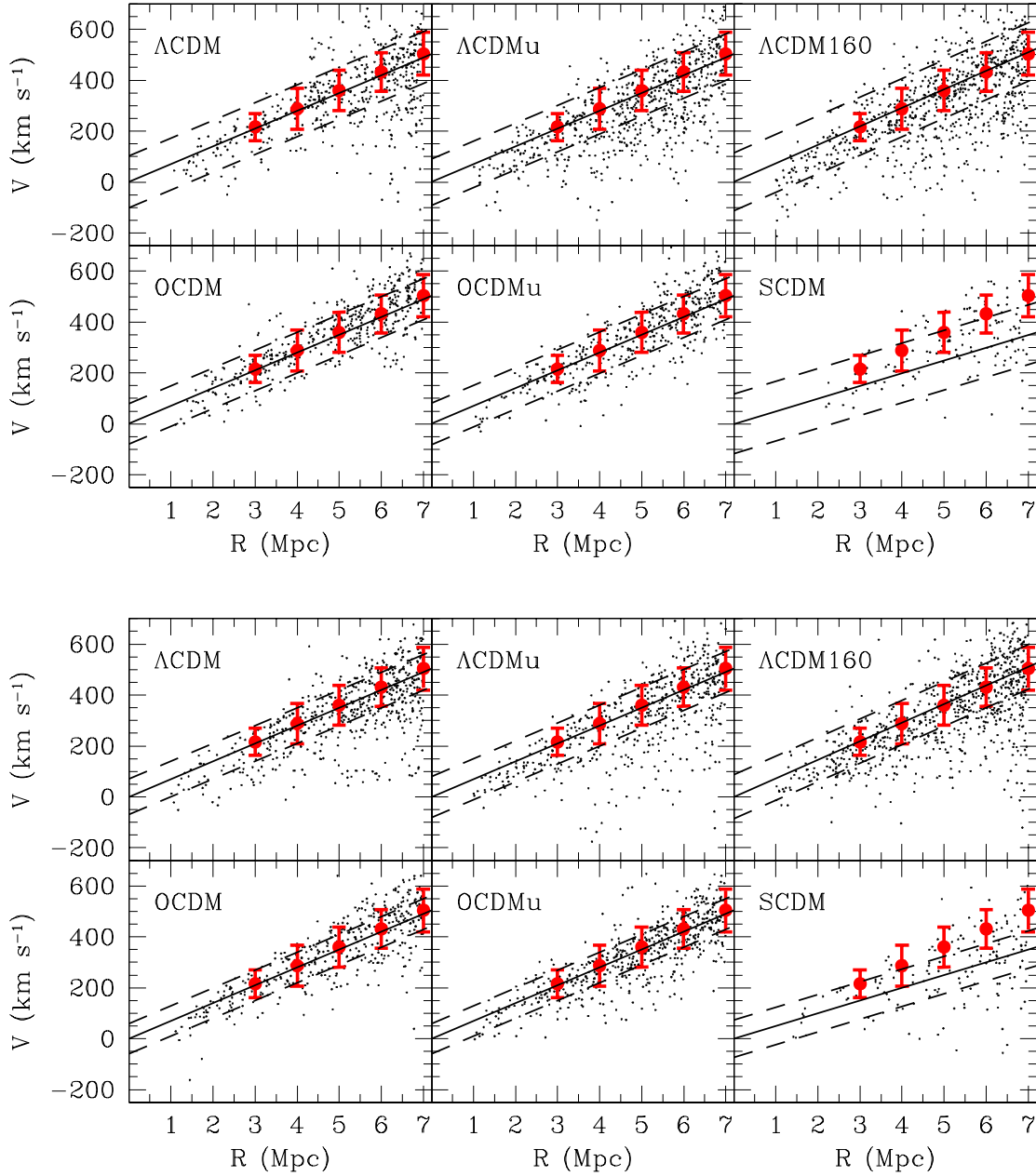


Figure 2. Combined Hubble diagrams of 10 randomly chosen LG-like objects in the different simulations. The solid lines represent the  $H_0 r$  Hubble flow and the dashed ones show the median of  $H_0$  (see Table 3). The individual data points (in red) correspond to the mean radial velocity and the  $H_0$  dispersion in the (1–R) Mpc distance cut of the Tikhonov & Klypin (2008) data. The upper panel presents the LG-like objects selected using the Pairs criterion and the lower ones correspond to those LG’s selected with the Singles.

| Criterion | CDM | CDM u | CDM hr | CDM 160 | OmegaCDM | OmegaCDM u | SCDM |    |    |    |    |    |     |    |
|-----------|-----|-------|--------|---------|----------|------------|------|----|----|----|----|----|-----|----|
| Pairs     | 102 | 40    | 91     | 47      | 90       | 60         | 114  | 58 | 80 | 25 | 81 | 30 | 117 | 33 |
| Singles   | 70  | 41    | 80     | 44      | 69       | 42         | 87   | 46 | 60 | 22 | 60 | 30 | 74  | 38 |

Table 3. The median of  $H_0$  (in  $\text{km s}^{-1}$  units) and the standard deviation from the median for all the LG candidates in each simulation selected with Pairs and Singles criteria (see Fig. 2).

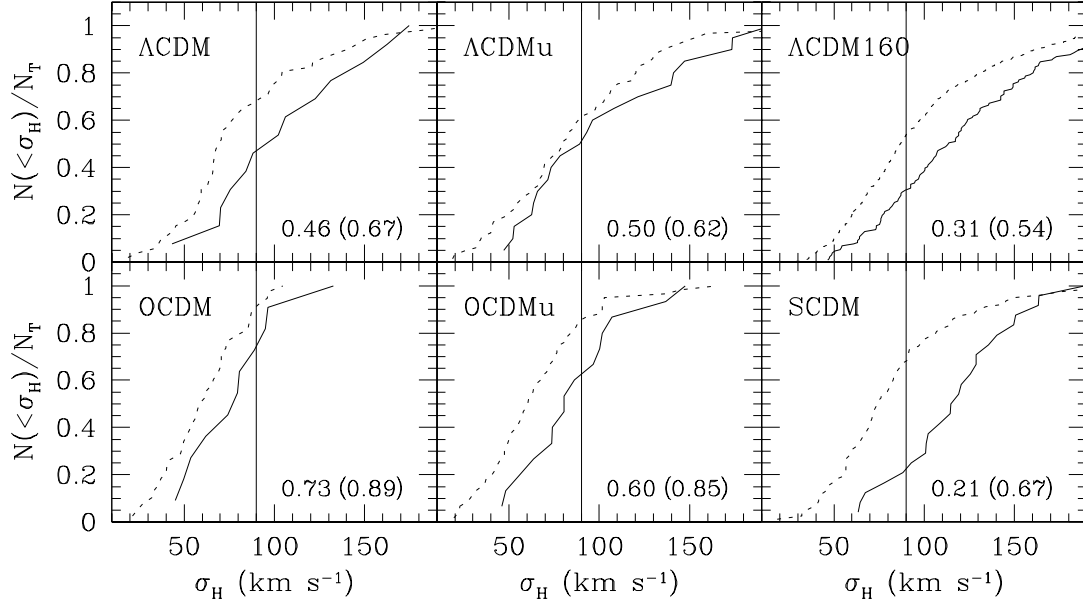


Figure 3. Cumulative number of LG candidates, from Pairs (solid lines) and Singles (dashed lines) criteria, with a  $\sigma_H$  lower than a given value, for the different simulations. The vertical line shows the value of the observational  $\sigma_H = 90.4 \text{ km s}^{-1}$ . The numbers on each frame are the fraction of LG-like objects with  $\sigma_H$  below this observational value for the Pairs and Singles (in parentheses).

|   | Distance between members (M pc) | No neighbours (M pc) | Virgo clusters | $\sigma_H$ (km s <sup>-1</sup> ) |
|---|---------------------------------|----------------------|----------------|----------------------------------|
| a | 1.0                             | 3                    | only one       | 102 40                           |
| b | singles                         | 3                    | only one       | 70 41                            |
| c | 1.5                             | 3                    | only one       | 85 47                            |
| d | 1.0                             | no constrain         | only one       | 189 100                          |
| e | 1.0                             | 5                    | only one       | 104 14                           |
| f | 1.0                             | 3                    | no constrain   | 113 112                          |
| g | 1.0                             | 3                    | one or more    | 150 74                           |

Table 4. The median of  $\sigma_H$  and the standard deviation from the median for the candidates in the  $\Lambda$ CDM simulation for different selection criteria (see text).

in x4. These are formulated in terms of the five criteria for the selection of LG-like objects. These dynamical properties are common in the Universe, yet the particular dynamical configuration of the LG determines  $\sigma_H$ . It is interesting to see how these properties affect the flow field around the LG and for that purpose we have relaxed some of the criteria of x4, reselected ensembles of mock LGs and studied the cumulative histogram of  $\sigma_H$  for the various selections (in the  $\Lambda$ CDM simulation). This is shown in Table 4 and Fig. 5, where the median and the cumulative fraction of LG-like objects of the constrained  $\Lambda$ CDM simulation, respectively, is shown for the following cases:

- (a) The Pairs, which are taken as a benchmark.
- (b) The case of Singles.
- (c) The Pairs criteria, but assuming a distance between LG members lower than 1.5M pc.
- (d) No constraint is imposed on the lack of nearby galactic size halos.

(e) There must not be objects similar to LG members within a distance of 5M pc.

(f) No constrained is imposed on the existence of a Virgo-like cluster.

(g) There must be one or more Virgo-like clusters.

The Pairs selection is taken here as a benchmark and it is represented here for the sake of completeness. The largest departure from the benchmark Pairs is obtained by removing the constraint on nearby LG-like objects (case d). Table 4 and Fig. 5 clearly show the role of clusters in heating the flow. A nearby Virgo-like cluster exerts a tidal field in the vicinity of the LG-like object, resulting in a shear flow which contributes to the anisotropic component of the velocity field and thereby heating the flow. The benchmark case (a) has only one Virgo-like cluster while in case (g) there can be one or more clusters. As expected, the flow for objects found in case (g) is significantly hotter than for those found following case (a). The removal of the Virgo constraint increases somewhat the median but it more than doubles the stan-

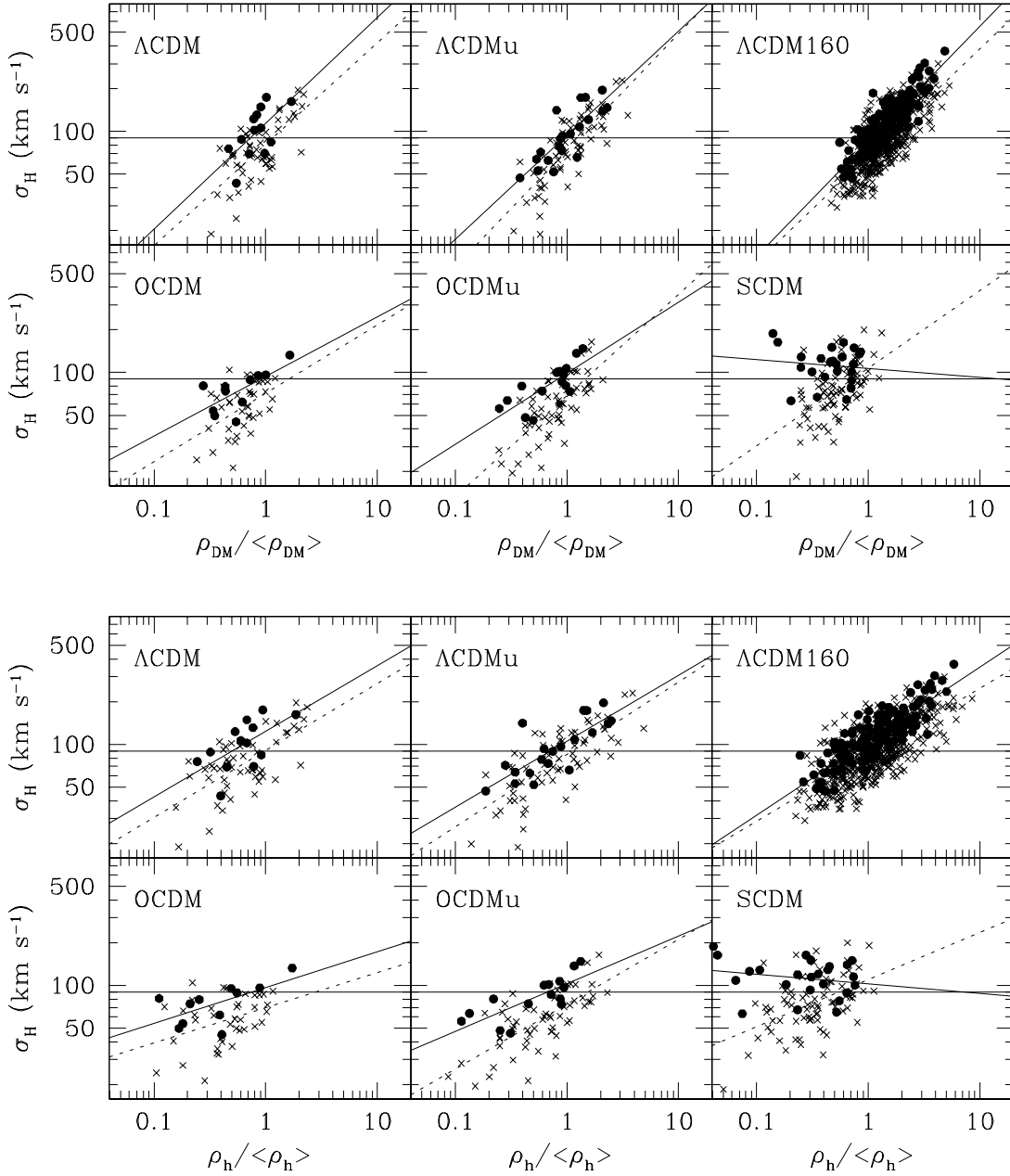


Figure 4. A scatter plot of the relation between  $\sigma_H$  and the mean matter density (normalized by the mean cosmological density) within the LV ( $R = 7Mpc$ ) for Pairs (solid points) and Singles (crosses). Power law fits to the  $\sigma_H$ -density scatter are shown for the Pairs (solid line) and Singles (dashed line). The horizontal line indicates the observational  $\sigma_H$ . In the upper panel the matter density is calculated from all DM particles inside the sphere. In the lower panel, the density is calculated from DM particles belonging to halos only.

standard deviation (case f). In such a case mock LGs can either have rich clusters within their LV, hence with very high  $\sigma_H$ , or can reside in low density regions far away from clusters and consequently have very low  $\sigma_H$ . Similarly, allowing for nearby MW size halos heats the low end and leads to many hot LG-like systems (case d). The analysis shows that the most significant selection criterion is that of the nearby halos (d). By only fitting this criterion only roughly 15% of the LG-like objects have  $\sigma_H$  smaller than the observed value.

## 7 MASS RESOLUTION

The numerical simulations used here span a mass resolution that ranges over more than two orders of magnitude. The majority of the simulations are done on a very coarse grid of  $256^3$  and have low mass resolution. In fact, the LG-like objects of the low resolution CDM and OCDM are made of about a thousand DM particles and the minimum mass of DM halos is  $3 \times 10^{10} h^{-1} M_\odot$ . The faint nearby galaxies



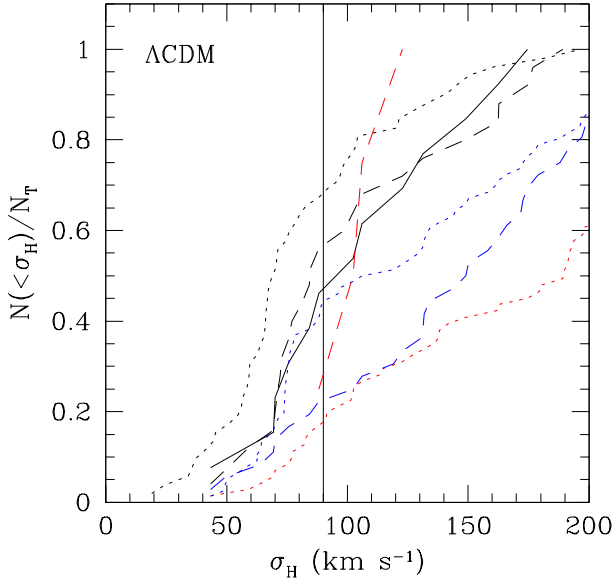


Figure 5. Fractional cumulative distribution of  $\sigma_H$  for the LG candidates in the  $\Lambda$ CDM simulation found with the different criteria shown in Table 4. The black lines correspond to a (solid), b (dotted) and c (dashed), the red ones to d (dotted) and e (dashed), and the blue ones to f (dotted) and g (dashed) criteria. The vertical line shows the value of the observational  $\sigma_H$ .

are presumably much less massive than this lower limit and the question arises as to what extent the present results are affected by the lack of resolution.

To address the issue of mass resolution we have analyzed the CDM hr simulation and compared it with the CDM one. This is a high resolution ( $N = 1024^3$ ) CDM (WMAP3) constrained simulation in the same  $64 h^{-1} Mpc$  volume. This simulation differs from the low resolution CDM one in terms of resolution, cosmological parameters and hence the power spectrum. It constitutes a different realization of the random field used to set the constrained initial conditions. An ensemble of LG-like objects has been constructed and  $\sigma_H$  has been calculated for all the DM halos in the corresponding LV (Figure 6, red curves) and for DM halos above the mass limit of the CDM simulation ( $3 \cdot 10^{10} h^{-1} M_\odot$ ; blue curves). These are compared with the cumulative distribution of the low resolution CDM simulation. Figure 6 shows very clearly that, within the range studied here, the distribution of  $\sigma_H$  does not depend on the mass resolution.

## 8 THE LOCAL VOLUME AND BLUESHIFTED GALAXIES

A striking manifestation of the coldness of the local flow is the absence of blueshifted galaxies in the local neighborhood. In particular the CNGB catalog shows only one blueshifted galaxy in the distance range of  $(1-7) Mpc$ , and it is flagged as a probable member of the Virgo, i.e. its distance might be erroneous. The absence of blueshifted galaxies provides only a qualitative measure for the coldness

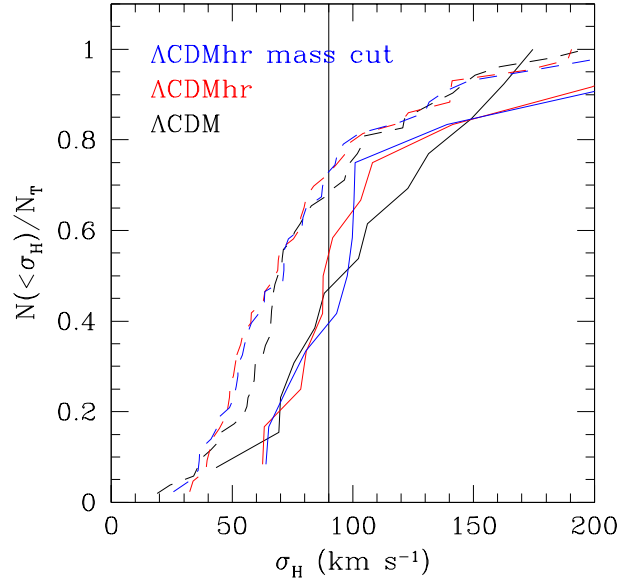


Figure 6. The fractional cumulative distribution ( $N(<\sigma_H)/N_T$ ), of LG candidates for simulations with different mass resolutions: The black curves correspond to the CDM simulation and the red ones to the CDM hr. The blue curves correspond to CDM hr, but using only halos within the LG's in the same mass limit than those in the CDM simulation. The solid lines correspond to the LG-like objects selected by the Pairs and the dashed ones to those selected by the Singles criteria. The vertical line shows the observational  $\sigma_H = 90.4 km s^{-1}$ .

of flow, yet it constitutes a very selective criterion for finding LG-like objects (Schlegel et al. 1994). The implications of such a selection on the coldness of the flow around the selected groups are studied here.

A word of caution is due before applying the constraint of no blueshifted 'galaxies' to the LG-like objects. Here, the local velocity field is traced by DM halos. It follows that the number of blueshifted objects might depend on the mass resolution of the simulations. We follow here Tikhonov & Klypin (2008) and assume that in the CDM model DM halos with  $V_{circ} > 35 km s^{-1}$  serve as proxy for observed luminous galaxies in the LV. Such halos are well resolved in the two high resolution simulations to which the no blueshifted 'galaxies' selection is applied. Table 5 lists the results of  $\sigma_H$  analysis applied to the

CDM hr and CDM 160 simulations. The analysis is applied to DM halos with  $V_{circ} > 35 km s^{-1}$ . The analysis is applied to all the LG-like objects and then to groups that contain no blueshifted galaxies in the shell corresponding to  $(x-7) Mpc$ , where  $x = 2; 3$  and  $5 Mpc$ . The Table lists the number of LG-like objects and the median and standard deviation of  $\sigma_H$  of the selected objects. Figure 7 shows the cumulative histogram of  $\sigma_H$  for the CDM hr and CDM 160 simulations. The figure presents the benchmark case of all pairs and the objects with no blueshifted  $V_{circ} > 35 km s^{-1}$  DM halos in the  $5 \{7 Mpc$  and  $3 \{7 Mpc$  shells. Figure 8 shows a scatter plot of  $\sigma_H$  against the mean density within the LV, for the same objects considered in Figure 7.

As expected, both Table 5 and Figure 7 show that the

constraint of no having blueshifted galaxies implies LG-like objects with cold environments. Both high-resolution simulations have yielded objects with no blueshifted galaxies. As can be deduced from Table 5, the closer to the LG we look for blueshifted galaxies, the less number of LG's pass the criterion. Given the uncertainties involved in the association of  $V_{\text{circ}} < 35 \text{ km s}^{-1}$  halos with nearby faint galaxies, we think that the number of LG-like objects with no blueshifted galaxies cannot be used as a reliable statistic of the local environment. Yet, it provides another strong observational evidence for the coldness of the local flow. Figure 8 provides further support to our earlier findings about the relation between  $v_H$  and the mean density of the LV (Figure 4). LG-like objects with no blueshifted 'galaxies' in their LV are cold,  $v_H < 100 \text{ km s}^{-1}$ , and they resides in LV with  $\rho_{\text{DM}} = \rho_{\text{DM}} \cdot 2$ .

## 9 DISCUSSION

A suite of CDM simulations have been used to study the nature of the velocity field around Local Group-like objects. The objects are selected so as to reproduce the main dynamical properties of the LG, which include the range of masses of the two most massive DM halos in the group, the proximity to a Virgo-like cluster and the absence of nearby massive halos. The flow field has been analyzed by means of  $v_H$ , which is defined by the RMS value of the residual from the pure Hubble flow, of all galaxies within the Local Volume, defined to be the volume enclosed within a radius of 7 Mpc around the LG. The results are compared with the  $v_H$  calculated for the CNG data. Two important conclusions are reached here. The first, and the more important one, is that there is no 'coldness of the local flow' problem, but rather it is the relation between  $v_H$  and the mean local matter density that needs to be addressed in the context of the LV. The other is that within the canonical CDM cosmological models  $v_H$  depends only on the mean matter density and not on the cosmological constant. Recently, Tikhonov et al. (2009) have found a similar cold flow around LG-like objects in a model with Warm Dark Matter (WDM) of 1 keV particle masses which leads to a cut-off in the power spectrum above  $k_{\text{peak}} = 3.7 h^{-1} \text{ Mpc}^{-1}$ .

The main result that has been found is that for all models considered here there is a non-negligible fraction of the LG-like objects with  $v_H$  close to the observed value. The two CDM simulations in the box  $64 h^{-1} \text{ Mpc}$  have about (30–45)%, the CDM 160 has 25%, the two  $\Lambda$ CDM simulations have roughly (50–65)% and even the SCDM model has 17%, of their (Pairs) LG-like objects colder than the observed value. However the scatter in  $v_H$  is not random but it correlates strongly with the mean matter density within the LV, with higher  $v_H$  expected for higher density. In the canonical CDM case a  $v_H < 100 \text{ km s}^{-1}$  implies that the mean LV density is less than twice mean cosmological density. This is also consistent with the requirement that there are no blueshifted galaxies in the LV around the LG. It follows that the old 'coldness of local flow' problem reappears as a potentially new problem, namely the local density-coldness relation. The recent compilation of the abundance of galaxies in the LV of Tikhonov & Klypin (2008) provides interesting results. These authors studied the lu-

minosity function of the galaxies in the CNG data and estimated the LV fractional density to be about  $1.4 \pm 0.17$  within  $R = 8 \text{ Mpc}$ . Using DM halos with  $V_{\text{circ}} > 35 \text{ km s}^{-1}$  as a proxy to luminous galaxies, the  $\Lambda$ CDM predicted density enhancement in the LV stands in good agreement with the observed value. The realization that  $v_H$  and the local density are closely connected provides another reminder to the fact that progress in understanding the local dynamics depends on a parallel advance in understanding galaxy formation.

It has been speculated that the coldness of the local flow is a manifestation of the dark energy, which dominates the mass-energy density of the universe (Baryshev et al. 2001, Chemin et al. 2004, 2007, Macciò et al. 2005). The basic argument behind that claim is that very locally the gravitational field is supposed to be dominated by the cosmological constant and hence the induced Hubble flow is expected to be cold. This claim has been refuted by Homann et al. (2008) who showed that within a local volume defined by  $0.75 \times 6 R \times 6.2 \text{ Mpc}$  the flow is dominated by the DM, regardless of the existence of a cosmological constant. Namely, the  $\Lambda$ CDM and CDM models yield virtually the same  $v_H$  within that volume. The current paper extends the numerical experiments and reinforces the results of Homann et al. (2008). That earlier work is extended to cover more simulations of higher resolution and the LV is defined to extend over  $1.6 \times 6.7 \text{ Mpc}$ .

The current work substantiate and gives justification to the theoretical arguments suggested by Homann et al. (2008) as to why dark energy does not dictates the local dynamics. The arguments on the role of the dark energy are all based on approximating the local dynamics by the monopole term, i.e. a gravitational field induced by an isolated point-like object. This would have implied a very tight correlation between  $v_H$  and the mean overdensity within the LV, contrary to the large scatter manifested by Figure 7. The arguments advocating the cooling of the local flow by the dark energy completely ignore the environmental effects on the flow. These effects are very clearly demonstrated in Table 4 which shows that  $v_H$  nearly doubles by removing from the benchmark criteria the constraint on the lack of MW-like halos within a sphere of 3 Mpc. The proximity of Virgo-like halos also changes the value of  $v_H$ . It follows that the dynamics of quasi-linear objects such as the LG cannot be properly modeled without a detailed accounting of environmental effects.

The present paper reaches radically different conclusions than those expressed in Macciò et al. (2005) concerning the role of the cosmological constant in shaping the dynamics of the LV. Yet, a close inspection shows that there is no technical disagreement between the two papers. We were careful to follow the selection criteria of LG-like objects of Macciò et al. (2005) and hence their CDM simulation can be directly compared with the present ones. In spite of the somewhat different value of the physical parameters of the CDM model used in the two papers the scatter of  $v_H$  and its dependence of the local density are in close agreement. A careful reading of Macciò et al. (2005) reveals that their statement concerning the role of the term is based on the comparison these authors did with the  $\Lambda$ CDM simulation of Gouvenato et al. (1997).

A careful comparison with the  $v_H - \rho$  relation of

| no negative velocity halos | CDM hr        |                   | CDM 160       |                   |
|----------------------------|---------------|-------------------|---------------|-------------------|
|                            | LG candidates | $\sigma_H$ median | LG candidates | $\sigma_H$ median |
| all                        | 12            | 97 61             | 131           | 115 58            |
| 5-7 M pc                   | 7             | 85 15             | 46            | 90 31             |
| 3-7 M pc                   | 4             | 85 16             | 15            | 95 31             |
| 2-7 M pc                   | 1             | 69 1              | 6             | 99 19             |

Table 5. The case of LG-like objects with no blueshifted galaxies: The left column presents the selection criteria of the LG-like objects: all – the benchmark Pairs, the following rows corresponds to LG-like objects with no blueshifted DM halos with  $V_{\text{circ}} > 35 \text{ km s}^{-1}$ , taken as a proxy to observed galaxies, within the respective shell. Each row provides the number of such groups and the median of  $\sigma_H$  and its standard deviation measured within their LV. The analysis was applied to the two high resolution simulations, CDM hr and CDM 160.

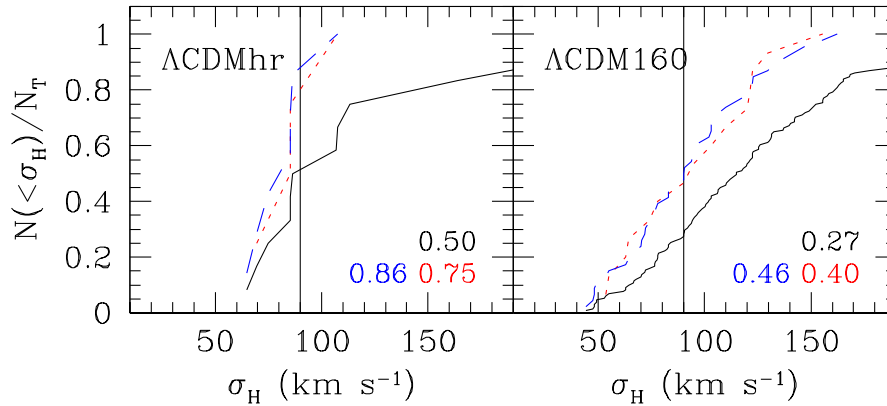


Figure 7. The Fractional cumulative distribution of LG candidates ( $N(<\sigma_H)/N_T$ ) for the two high resolution CDM hr (left) and CDM 160 (right) simulations. the solid line corresponds to the Pairs criterion, the other two lines represents groups with no blueshifted DM halos with  $V_{\text{circ}} > 35 \text{ km s}^{-1}$  within 5 (7 M pc (red-dotted) and 3 (7 M pc (blue-dashed) shells. The vertical line shows the observational  $\sigma_H = 90.4 \text{ km s}^{-1}$ .

the LG candidates in the  $\Lambda$ CDM simulation shown in Fig. 11 of Governato et al. (1997), and its presentation in Fig. 2 of Maccio et al. 2005, reveals that it can be reproduced in the present  $\Lambda$ CDM simulations by omitting the Virgo constraints on the selection of the LG-like objects. Given the present much better resolution, the number of our LG candidates is considerable larger than in Governato et al. (1997), in particular in the densest environments. The linear fit shown in Fig. 11 of Governato et al. is biased towards the LGs located in  $\sigma_H = 61$ , where most of their LGs are found. Restricting our fit to LGs with  $\sigma_H = 61$ , a quite similar fit emerges. This indicates that the old and present  $\Lambda$ CDM simulations equally reproduce, to within their resolution limits, the same kind of LG candidates. To summarize, by neglecting the Virgo constraints on the selection of LG-like objects and by restricting the analysis to less dense objects the old  $\Lambda$ CDM results are recovered. This might hint that the  $\Lambda$ CDM  $\sigma_H$  analysis of Governato et al. (1997) was performed with respect to their ‘cat2’ catalog rather than the stated ‘cat3’ catalog, in which the Virgo constraints were imposed.

No substantial differences are found between the constrained and unconstrained simulations. The constraints imposed here are affecting the structure on scales larger than 5 h<sup>-1</sup> M pc (Klypin et al. 2003), a scale that coincides with the LV. This implies that the behavior of  $\sigma_H$  predominantly

depends on the internal dynamics within the LV and less on the one induced by larger scales. This also gives further support to the claim that, apart from the particularities of the very nearby structure, the universe around us constitutes a very typical realization of the CDM cosmologies. The particular dynamical attributes of the LG are its mass range of about  $10^{12} h^{-1} M_\odot$ , its binary nature, the proximity to the Virgo cluster and the absence of similar nearby objects. These have been used as the selection criteria of LG-like objects in the simulations. In  $\Lambda$ CDM these criteria have been relaxed, while keeping the mass to be roughly the LG mass. One expects that the proximity of the Virgo cluster heats the flow field in the vicinity of the LG, due to its tidal field which induces non-isotropic motions around the LG. Hence the relaxation of the condition for a nearby Virgo-like cluster leads to colder LG-like objects. Similarly, in LG-like objects with a single MW-like halo the gravitational field is dominated by a monopole term and this leads to a colder flow than in binary LG-like systems. On the other hand the largest, yet opposite, effect is introduced by allowing MW-like halos to be close to the LG. The presence of such nearby halos heats the flow considerably. It follows that the main ingredient that is responsible for the coldness of the local flow is the relative isolation, and therefore also the low mean local density, of the LG. Furthermore, in the CDM cosmologies the coldness of the local flow depends more on the properties

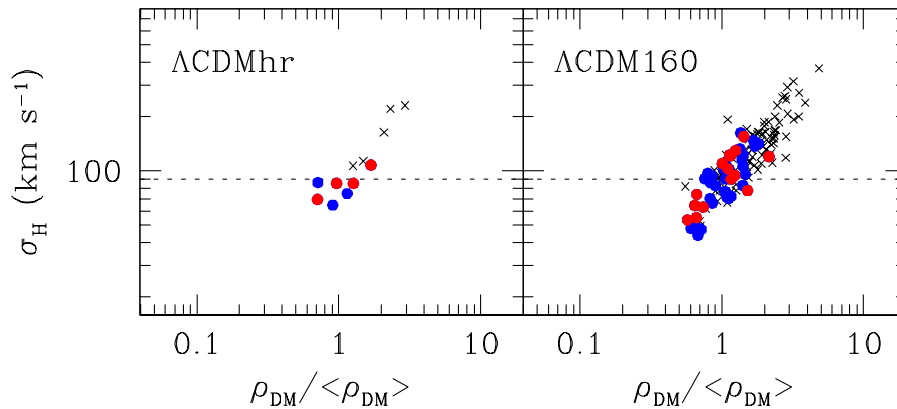


Figure 8. Scatter plots of  $\sigma_H$  vs. the mean matter density, normalized by the mean cosmological density, within the LV's found in the high resolution simulations,  $\Lambda$ CDMhr (left) and  $\Lambda$ CDM160 (right). All symbols correspond to LV's around LG-like objects found with the Pairs criterion in both simulations. The filled circles represent LV's with no blueshifted DM halos with  $V_{\text{circ}} > 35 \text{ km s}^{-1}$  within the  $5 \times 7 \text{ Mpc}$  shell (blue) and within  $3 \times 7 \text{ Mpc}$  shell (red). The crosses are for the rest of the LV's.

of the LG than on the possible presence of a dark energy component.

## 10 ACKNOWLEDGEMENTS

Fruitful discussions and correspondence with I. D. Karachentsev, A. Klypin, A. Maccio and A. Tikhonov are gratefully acknowledged. This research has been supported by the ISF (13/08 at the HU). The support of the European Science Foundation through the ASTROSIM Exchange Visits Program is acknowledged (SG, YH). The simulations were performed and analyzed on the Leibniz Rechenzentrum Munch (LRZ), the Barcelona Supercomputing Center (BSC) and the Magerit supercomputer at the Centro de Supercomputación y Visualización de Madrid (CeSVMA). SG acknowledges a Schonbrunn Fellowship at the Hebrew University Jerusalem. GY would like to thank also MEC (Spain) for financial support under project numbers FPA2006-01105 and AYA2006-15492-C03. LAMV acknowledges financial support from Comunidad de Madrid through a PhD fellowship.

## REFERENCES

- Baryshev Y. V., Chemin A. D., Teerikorpi P., 2001, *A & A*, 378, 729
- Chemin, A. D., Karachentsev, I. D., Teerikorpi, P., Valtonen, M. J., Byrd, G. G., Efremov, Y. N., Dolgachev, V. P., Domozhilova, L. M., Mkarov, D. I., & Baryshev, Y. V. 2007, *arXiv e-prints*, 0706.4068
- Chemin, A. D., Karachentsev, I. D., Valtonen, M. J., Dolgachev, V. P., Domozhilova, L. M., & Mkarov, D. I. 2004, *A & A*, 415, 19
- Davis M., Peebles P. J. E., 1983, *ApJ*, 267, 465
- Freedman W. L., Madore B. F., Gibson B. K., Ferrarese L., Kelson D. D., Sakai S., Mould J. R., Kennicutt Jr. R. C., Ford H. C., Graham J. A., Huchra J. P., Hughes S. M. G., Illingworth G. D., Macri L. M., Stetson P. B., 2001, *ApJ*, 553, 47
- Gill S. P. D., Knebe A., Gibson B. K., 2004, *MNRAS*, 351, 399
- Gottlber S., Klypin A., 2008, in Wagner, S. and Steinmetz, M. and Bode, A. and Behrm, M. ed., *High Performance Computing in Science and Engineering, The ART of Cosmological Simulations*. Springer-Verlag, p. 29
- Governato F., Moore B., Cen R., Stadel J., Lake G., Quinn T., 1997, *New Astronomy*, 2, 91
- Homan Y., Martinez-Vaquero L. A., Yepes G., Gottlber S., 2008, *MNRAS*, 386, 390
- Karachentsev I. D., Karachentseva V. E., Huchtmeier W. K., Mkarov D. I., 2004, *AJ*, 127, 2031
- Karachentsev I. D., Mkarov D. I., Sharina M. E., Dolphin A. E., Rebel E. K., Geisler D., Guhathakurta P., Hodge P. W., Karachentseva V. E., Sarajedini A., Seitzer P., 2003, *A & A*, 398, 479
- Karachentsev I. D., Kashibadze O. G., Mkarov D. I., Tully R. B., 2009, *MNRAS*, 393, 1265
- Klypin A., Gottlber S., Ravevsov A. V., Khokhlov A. M., 1999, *ApJ*, 516, 530
- Klypin A., Homan Y., Ravevsov A. V., Gottlber S., 2003, *ApJ*, 596, 19
- Ravevsov A. V., Klypin A., Homan Y., 2002, *ApJ*, 571, 563
- Maccio A. V., Governato F., Horellou C., 2005, *MNRAS*, 359, 941
- Martinez-Vaquero L. A., Yepes G., Homan Y., 2007, *MNRAS*, 378, 1601
- Reiprich T. H., Bohringer H., 2002, *ApJ*, 567, 716
- Sandage A., Tammann G. A., 1975, *ApJ*, 196, 313
- Sandage A., Tammann G. A., Hardy E., 1972, *ApJ*, 172, 253
- Schlegel D., Davis M., Summers F., Holtzman J. A., 1994, *ApJ*, 427, 527
- Spergel, D. N., et al. 2007, *ApJS*, 170, 377
- Spergel, D. N., et al. 2003, *ApJS*, 148, 175
- Springel V., 2005, *MNRAS*, 364, 1105
- Tikhonov A., Karachentsev I. D., 2006, *ApJ*, 653, 969
- Tikhonov A., Klypin A., 2008, *arXiv e-prints*, 0807.0924
- Tikhonov, A. V., Gottlber, S., Yepes, G., Homan, Y., in preparation, (2009)

- Tonry J. L., Dressler A., Blakeslee J. P., Ajhar E. A., Fletcher A. B., Luppino G. A., Metzger M. R., Moore C. B., 2001, *ApJ*, 546, 681
- Tully R. B., Shaya E. J., Pierce M. J., 1992, *ApJS*, 80, 479
- Willick J. A., Courteau S., Faber S. M., Burstein D., Dekel A., Strauss M. A., 1997, *ApJ*, 109, 333
- Zaroubi S., Ho man Y., Dekel A., 1999, *ApJ*, 520, 413